Tribology International 97 (2016) 71–76

Contents lists available at ScienceDirect

Tribology International

journal homepage: www.elsevier.com/locate/triboint

Hertzian load–displacement relation holds for spherical indentation on soft elastic solids undergoing large deformations

Chen-En Wu [a], Keng-Hui Lin [b], Jia-Yang Juang [a,*]

[a] Department of Mechanical Engineering, National Taiwan University, Taipei 10617, Taiwan
[b] Institute of Physics, Academia Sinica, Taipei 11529, Taiwan

ARTICLE INFO

Article history:
Received 3 November 2015
Received in revised form
20 December 2015
Accepted 23 December 2015
Available online 12 January 2016

Keywords:
Hertz contact theory
Nanoindentation
Soft materials

ABSTRACT

In this paper we investigate the validity of the Hertz theory at very large deformations by performing rigid spherical indentation on soft, linearly elastic silicone substrates using nanoindentation tests and finite element method. We show that the theory significantly underestimates and overestimates the contact radius and maximum contact pressure, respectively, as the ratio of indenter displacement δ to the indenter radius R exceeds 0.1. However, the loading load–displacement relation still holds ($<3\%$ discrepancy) for δ/R as large as 0.66 with a maximum principal strain of 46.6%. This agreement arises from a near cancellation of two non-Hertzian effects: the spherical (as opposed to paraboloidal) shape of the indenter, and the large deformation behavior of the linear elastic system. Our simulation results show that the Hertzian load–displacement relation does not hold for thin films where the ratio of thickness H to R is smaller than 20. We also consider rigid indentation on an elastic sphere with a radius of kR, and reveal that the elastic sphere is large enough to be treated as a half-space for $k>10$. Our results may provide practical guidelines to proper sample preparation and better interpretation of indentation data of elastic soft elastomers and gels.

1. Introduction

Contacts between deformable solids are ubiquitous in nature and engineering, and have important roles in various fields and applications from physics [1,2], biology [3,4], agriculture [5] and astrophysics [6] to nanoindentation [7,8], powders [9], magnetic disk drives [10] and railways [11]. The Hertz theory has been the cornerstone of modern contact mechanics since Hertz published his classic paper in 1882 [12]. It describes the normal contact between two perfectly elastic solids, and has been successful in predicting the load–displacement relation as well as other parameters such as contact radius and contact pressure. The theory uses parabolic approximation for the profile of the sphere, which is only valid for small contact radii. As a result, one of the major assumptions of the theory is small deformation, i.e. the contact area is generally small compared with the contacting bodies themselves [12–17].

The nanoindentation technique has become an important means to measure mechanical properties of soft and biological materials including cells [18], soft elastomers and gels [19]. Whereas the Hertz theory was originally developed to describe macroscopic contacts with infinitesimal strain, it has been widely applied to interpret the indentation data of soft materials where the deformation is often not small or the sample thickness is in the nanometer to micrometer regime [19]. It has been shown that shallow depth indentation often suffers from excessive noise which may preclude the accuracy of the measurement [7]. Relative larger indentation depth can help reduce the measurement noise due to surface effects, but the interpretation of the data become more challenging.

There is a wealth of literature on the applicability of the Hertz theory to the interpretation of indentation data. Many have focused on elastic–plastic problems of metallic solids [7,20], which show a reversible linear elastic behavior only to 1% of the strain. Dintwa et al. [21] investigated the validity of the Hertz theory, for two contacting elastic spheres and contact of an elastic sphere on a rigid flat, using finite element method (FEM), and concluded that large strains cause important prediction errors in the Hertz theory – for both cases the Hertz model systematically underestimates the normal force even at a relative small indentation. Yoffe [22] published pioneering theoretical work on the modification of Hertz theory for spherical indentation for wider contact. Lim et al. [23] carried out pioneering experimental work on PDMS and other rubbers using 4-mm diameter spherical indenter. They confirmed that the experimental loading curves were well fitted by the Hertz equation with a δ/R up to 0.15, where R is the indenter radius and δ the indenter displacement. A large amount of work has been carried out on the indentation of soft solids considering material

* Corresponding author.
E-mail address: jiayang@ntu.edu.tw (J.-Y. Juang).

http://dx.doi.org/10.1016/j.triboint.2015.12.034
0301-679X/

nonlinearity such as hyperelasticity [13,15,24–27], viscoelasticity [28,29] and poroelasticity [30]. Most of the work focused on the identification of the nonlinear material properties or the constitutive parameters from fitting measured load–displacement data using inverse methods. Although these nonlinear models are comprehensive and provide insight into the nature of soft materials, the inverse method often requires a numerical optimization procedure [26] in contrast to the Hertzian theory by which the Young's modulus can be readily obtained. Accordingly, the Hertzian load–displacement curve is still widely used by researchers to extract the Young's modulus [19] without knowing the level of accuracy. Recently Nalam et al. [31] measured local material properties of hydrogels using colloid-attached atomic force microscope probes ($R=2.5\ \mu m$) in liquid with a maximum indentation depth of 350 nm. During the loading process at low frequencies, their measured force-indentation relation agreed with the Hertz model, and the load was not affected by interfacial bonding during approach. Despite the extensive work, the applicability of the Hertzian theory for very large indentation ($\delta/R=1$) remains unclear, and a better quantitative understanding and a direct comparison between the theory, experiment, and numerical simulation are still lacking.

Here we quantify the extent of deviation from the Hertzian theory which result from geometrical nonlinearities in the large strain regime by performing rigid spherical indentation on soft, linearly elastic silicone substrates using nanoindentation tests and finite element method. Material properties are directly measured by tensile tests, instead of by fitting the indentation data, to avoid any additional uncertainty.

Fig. 1 shows a schematic of the contact between a rigid spherical indenter and a deformed elastic half-space as a result of a normal load F. The half-space is assumed perfectly elastic, homogeneous and isotropic. Hertz approximated the original separation between the axisymmetric contacting bodies by $z=(x^2+y^2)/2R=r^2/2R$, where r is the radial coordinate, z the axis of symmetry and x–y the common tangent plane of the two bodies. Hertz also proposed the contact pressure distribution p of the circular contact as $p=p_0\ [1-(r/a)^2]^{1/2}$, where a is the contact radius, p_0 the maximum contact pressure on the surface and it occurs at the center. The maximum pressure is given by $p_0=3F/2\pi a^2$, where F is the normal load. The well-known Hertzian relationship between the load F and displacement δ is given by

$$F=\frac{4}{3}E^*R^{0.5}\delta^{1.5} \tag{1}$$

where $E^*=E/(1-\nu^2)$ is the equivalent elastic modulus, E and ν are the Young's modulus and Poisson's ratio of the elastic half-space, respectively.

2. Experimental

Some silicone gels and elastomers [32–34] are known to exhibit linearly elastic behavior at a strain larger than 20%, and are suitable as the test material for this work. We prepared polydimethylsiloxane (PDMS, Sylgard 184, Dow Corning), a silicone elastomer, following an existing protocol [34]. It was prepared by mixing an elastomer base and a cross-linker at a weight ratio of 10:1 for 10 min with a spatula, followed by degassing. The prepolymerized mixture was then poured into a mold, degassed, and then cured at 80 °C for 24 h. After the hardening process, the sample was taken out of the mold and glued to two acrylic clamps, resulting in specimens measuring $60.0\times 20.0\times 3.0\ mm^3$ and the rectangular test section measuring $25\times 20.0\ mm^2$. All tensile tests were performed in air, at room temperature, using a tensile machine (Criterion 42.503 Test System, MTS) in the displacement-controlled mode at a constant rate of 0.5 mm/min. We use camera (D90, Nikon) with micro lens (AF-S MICRO NIKKOR 105 mm 1:2.8 G ED, Nikon) to take images of the test section at the center of the sample during the test (Fig.2).

The stress–strain curve is obtained using the test section, and hence the effect of the instant glue and acrylic clamps can be excluded. We confirmed that test section can be regarded as under uniaxial tension by finite element simulations. Fig. 2(c) shows the stress–strain curves and the Poisson's ratio as a function of the tensile strain ε_y. The Poisson's ratio, $\nu=0.412\pm 0.00924$, was calculated as the ratio of transverse strain ε_x and tensile strain ε_y, which were estimated from the images of the test section. For $\varepsilon_y<0.05$ the transverse strain ε_x was too small to resolve reliably using our experimental setup so the Poisson's ratio was not

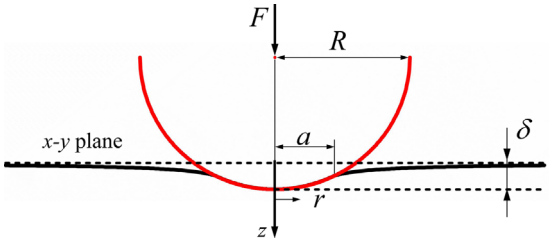

Fig. 1. Schematic diagram of the spherical indentation.

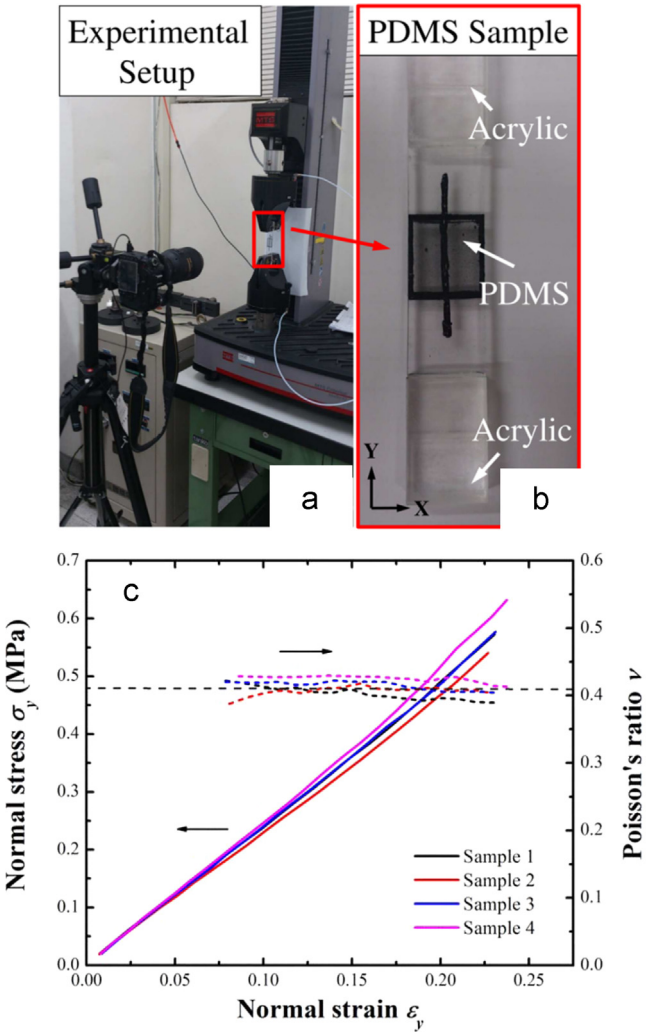

Fig. 2. (a) Experimental setup and (b) PDMS sample for our tensile test. (c) The measured stress-strain curves and Poisson's ratios. The stress is calculated by P/A, where P is the applied load, and A is the measured cross-sectional area of the deformed test section. The Young's modulus and Poisson's ratio are 2.463 ± 0.117 MPa and 0.412 ± 0.00924, respectively.

measured for $\varepsilon_y < 0.05$ and was assumed to be constant. The stress was calculated as P/A, where P is the applied load, A the measured cross-sectional area of the deformed test section. The stress–strain curves show negligible nonlinearity with a ε_y up to 23%. The Young's modulus E was 2.463 ± 0.117 MPa. The measured E and ν were used as the material properties for the FEM simulations and Eq. (1).

Nanoindentation tests were performed using nanoindenter (TI 950 TriboIndenter, Hysitron) with a conical sapphire indenter. The nominal radius of the tip R is 5 μm and the included angle is 60 °. The displacement resolution is < 0.02 nm, and the load resolution is < 1 nN. A triangular loading function was used in the nanoindentation tests with loading and unloading rates equal to 0.1 μm/s. The dimension of the PDMS sample was $10 \times 10 \times 4$ mm^3.

3. Finite element analysis

We simulate the rigid spherical indentation on three different substrates: (1) a half-space, (2) a substrate with finite thickness, and (3) a sphere, by using the finite element package ANSYS. An axisymmetric finite element model is created including a rigid spherical indenter pressing into an elastic substrate. The minimum element size is 0.0375 R. For the case of elastic half-space, the thickness H and radius of the substrate is 20 R and 12 R, respectively. Numerical results are insensitive to further increase of the dimension of the substrate or the refinement of the mesh. Hence the model can be regarded as a half-space. The bottom of the substrate is fixed, and the top surface outside the contact is traction-free. The rigid indenter moves only in the vertical direction. The substrate is assumed linearly elastic, homogenous and isotropic with the material properties, E and ν, measured by the tensile test. The load–displacement curve is obtained by prescribed-displacement static simulations in which the indenter is pressed into the substrate at prescribed depths up to $\delta = R$, and the applied load F required for static equilibrium is calculated. Geometric nonlinearity, such as large rotation and large strain, is included. The contact between the indenter and the substrate is assumed to be frictionless. Fig. 3 shows a representative finite element mesh and the maximum principal strain field in our simulations ($\delta = 3$ μm and $R = 5$ μm). The maximum strain is 43.6% at $z = 1.12$ μm.

4. Results and discussion

Fig. 4 shows a comparison of the dimensionless load F/E^*R^2 versus dimensionless displacement δ/R between the FEM, indentation data, and Eq. (1). The three indentation data were conducted at different locations on the sample. Eq. (1) shows remarkable agreement with the FEM and indentation data even at large indentations. For a deviation of 3% in load, δ/R is 0.66 and 0.57 for the FEM and indentation data, respectively. At $\delta/R = 0.66$ the corresponding dimensionless contact radius a/R and the maximum principal strain ε, both calculated by FEM, are 0.74 and 46.6%, respectively (Fig.4). The measured loads are slightly smaller than the FEM predicts at very large indentations (~5% smaller at $\delta/R = 0.80$), which is most likely because the PDMS can no longer be assumed linearly elastic at such large strains (55%). The three experimental curves overlap and show a hysteresis, indicating occurrence of plastic deformation in PDMS with a small residual depth of 0.25 μm. Eq. (1), FEM and indentation data show excellent agreement for $\delta/R < 0.60$. This reassuring observation is rather surprising since this value of δ/R corresponds to strains in the contact region rising to about 44%.

Indentation of a soft PDMS substrate, especially at the nanoscale depth, may involve adhesive effect [35]. We consider the total adhesion energy at the indenter-sample interface as $U_{adh} = W A_c$, where W is the adhesion energy per unit area associated with the contact, and A_c is the contact area. The value of W depends on the contacting materials, which has been measured to be 42.5 and 110 mN/m for PDMS/PDMS and PDMS/Si interface, respectively [35,36]. In our case, at an indentation depth of $\delta = 1$ μm ($\delta/R = 0.2$), the contact area $A_c = 4.62$ μm^2 and $F = 15$ μN. The adhesion energy U_{adh} is estimated between 6.2×10^{-13} and 1.6×10^{-12} J, whereas the elastic strain energy stored in the PDMS is estimated to be 7.5×10^{-12} J, indicating that the elastic energy is significantly larger than that of the adhesion energy for larger indentations. Also, no adhesion force (pull-off force) was measured when the indenter separated from the PDMS during the unloading process. Accordingly, the adhesive effect may be negligible in our study.

In order to understand why the Hertzian load–displacement relation still holds for large indentations and strains, we plotted the surface profiles of the indenter and the deformed half-spaces at different δ/R in Fig. 5(a). The black dash is the profile of the rigid

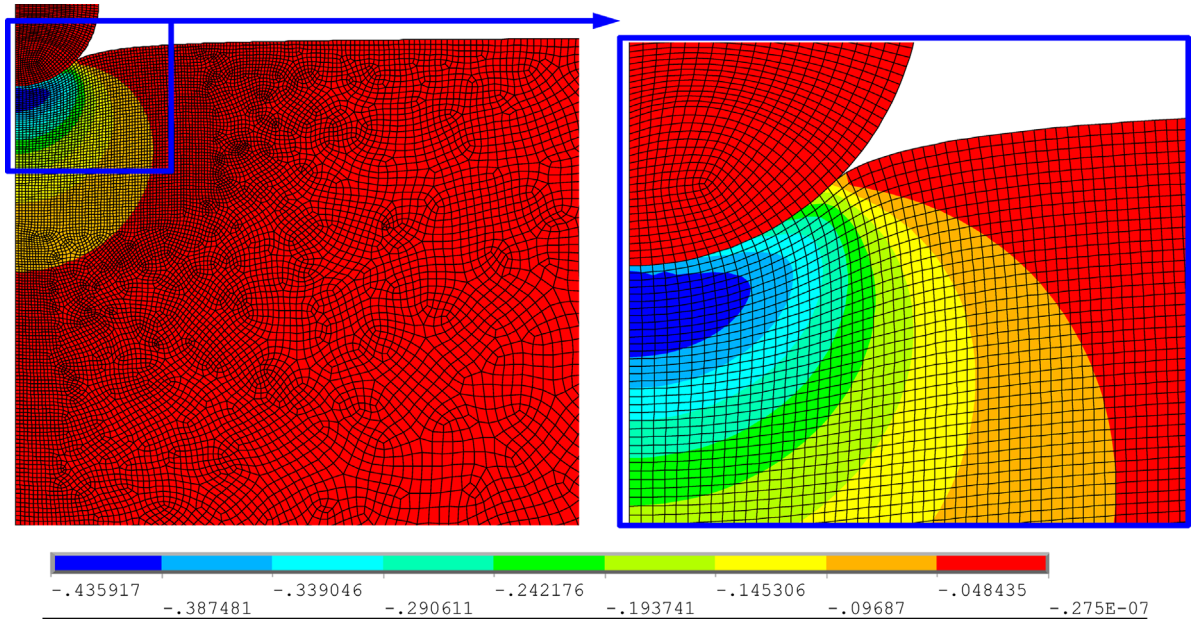

Fig. 3. Representative finite element mesh and the maximum principal strain field in our simulations. ($\delta = 3$ μm and $R = 5$ μm.) The maximum strain is 43.6% (compressive) at $z = 1.12$ μm.

sphere and the black solid is a paraboloid Hertz used to approximate the sphere. Other curves are profiles of the indented elastic half-space in which the solids and dashes are given by Hertz and FEM, respectively. As $\delta/R <$ 0.2, the profiles of Hertz and FEM coincide with each other, indicating that the paraboloid approximates the sphere well. The profiles, however, deviate from each other as $\delta/R >$ 0.2 (or $a/R >$ 0.43), and hence the paraboloid can no longer approximate the sphere. The contact area predicted by the Hertz theory is much larger than that of the FEM at larger indentations. This is one of the reasons the Hertz theory is, in general, only valid for small indentation.

Fig. 5(b) shows dimensionless contact pressure distributions σ_z/E from $\delta/R = 0.01$ to $\delta/R = 1$. The distributions of FEM agree well with those of Hertz for $\delta/R <$ 0.2, which is consistent with the results of surface profile in Fig. 5(a). For $\delta/R >$ 0.2, the Hertz theory overestimates the contact radius, and underestimates the maximum contact pressure. Although the pressure distribution predicted by the Hertz theory is quite different from the more realistic one calculated by the FEM, its resultant, obtained by integrating the contact pressure over the contact area, happens to be very close to that obtained by the FEM for $\delta/R <$ 0.66 as shown in Fig. 4. Their difference in load becomes larger for $\delta/R >$ 0.66 (5.8% at $\delta/R=1$). We performed the FEM simulations using different elastic moduli ($10E$ and $0.1E$) and indenter radii (10 R and 0.1 R), and confirmed that the dimensionless load and contact radius versus indenter displacement as shown in Fig. 6(a) are very close to the original case in Fig. 4, meaning that the conclusion is valid regardless of the Young's modulus of the half-space and indenter radius.

The Hertz theory assumes that the interface is frictionless, but it is unlikely the case for the experimental conditions. Here we assess this effect by comparing the load–displacement curves between Eq. (1), frictionless contact interface (FEM), and "bonded" contact interface (FEM) as shown in Fig. 7. In the bonded contact interface case, the two contacting surfaces are bonded in all directions (once contact is established) for the remainder of the analysis. We found that whether frictionless or bonded, the interface only has minimum effect on the loading curve, which suggests our results still hold regardless of the local friction coefficient.

Indentation test is also widely used to measure the mechanical properties of thin films with finite thickness [19,37]. However, when the substrate is no longer an elastic half-space, the rigid support to which the film is attached may influence the measurement of load–displacement curves. As a result the Young's modulus extracted from such curves often appears stiffer than its actual value, known as the "substrate effect" [37] (the substrate here refers to the rigid support instead of the film). Fig. 6(b) shows the dimensionless load–displacement curves with different ratios of substrate thickness H and indenter radius R. The curves of $H/R=20$, used in previous models, and $H/R=100$ are very close, indicating that $H/R=20$ can be considered as a half-space. The dimensionless load increases as H/R decreases for $H/R <$ 20 due to the rigid support. It is interesting that the curve $H/R=12$ has good agreement with Eq. (1) with a deviation less than 3% over the entire depth. This intriguing phenomenon may be explained as follows: At $H/R=12$, the rigid support does not affect the contact behavior when δ/R is under 0.66. However, as δ/R is larger than 0.66 – indentation exceeds 5.5% of the film thickness – the rigid support begins to affect the contact behavior, resulting in a larger maximum contact pressure and load. The stiffening due to the rigid support compensates the overestimate in load by Eq. (1), resulting in the good match of the load–displacement curves. The contacting bodies are assumed semi-infinite in the Hertz theory so Eq. (1) does not include any effect due to the rigid support. If we further reduce the film thickness, the load increases significantly, and the Young's modulus obtained according to Eq. (1) may be substantially overestimated. The "extreme hardening" of PDMS films observed by Xu et al. [19] may indeed due to the effect of rigid support.

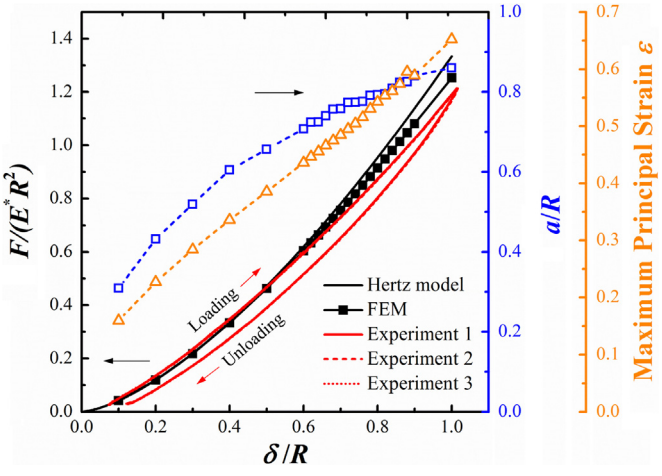

Fig. 4. Comparison of the dimensionless load, contact radius, and maximum principal strain versus dimensionless displacement between Eq. (1), FEM, and indentation data. The three experiments were conducted at different locations. The material properties used in Eq. (1) and the FEM were measured by the tensile test. No fitting parameters were used here.

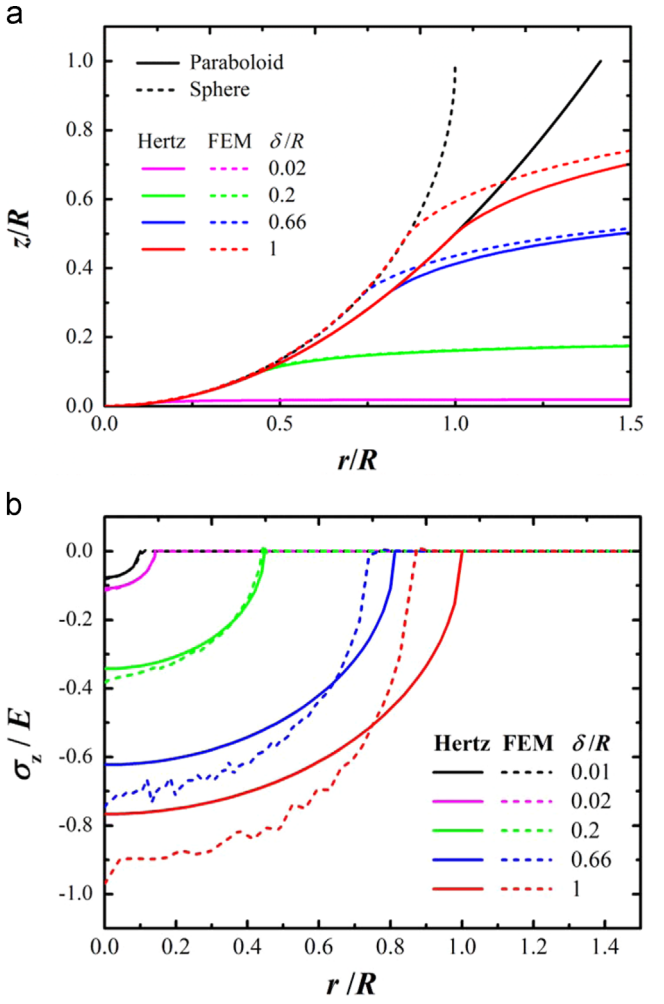

Fig. 5. (a) Surface indentation profiles at various depths. (b) Comparison of dimensionless contact pressure and contact radius between the Hertz theory and FEM.

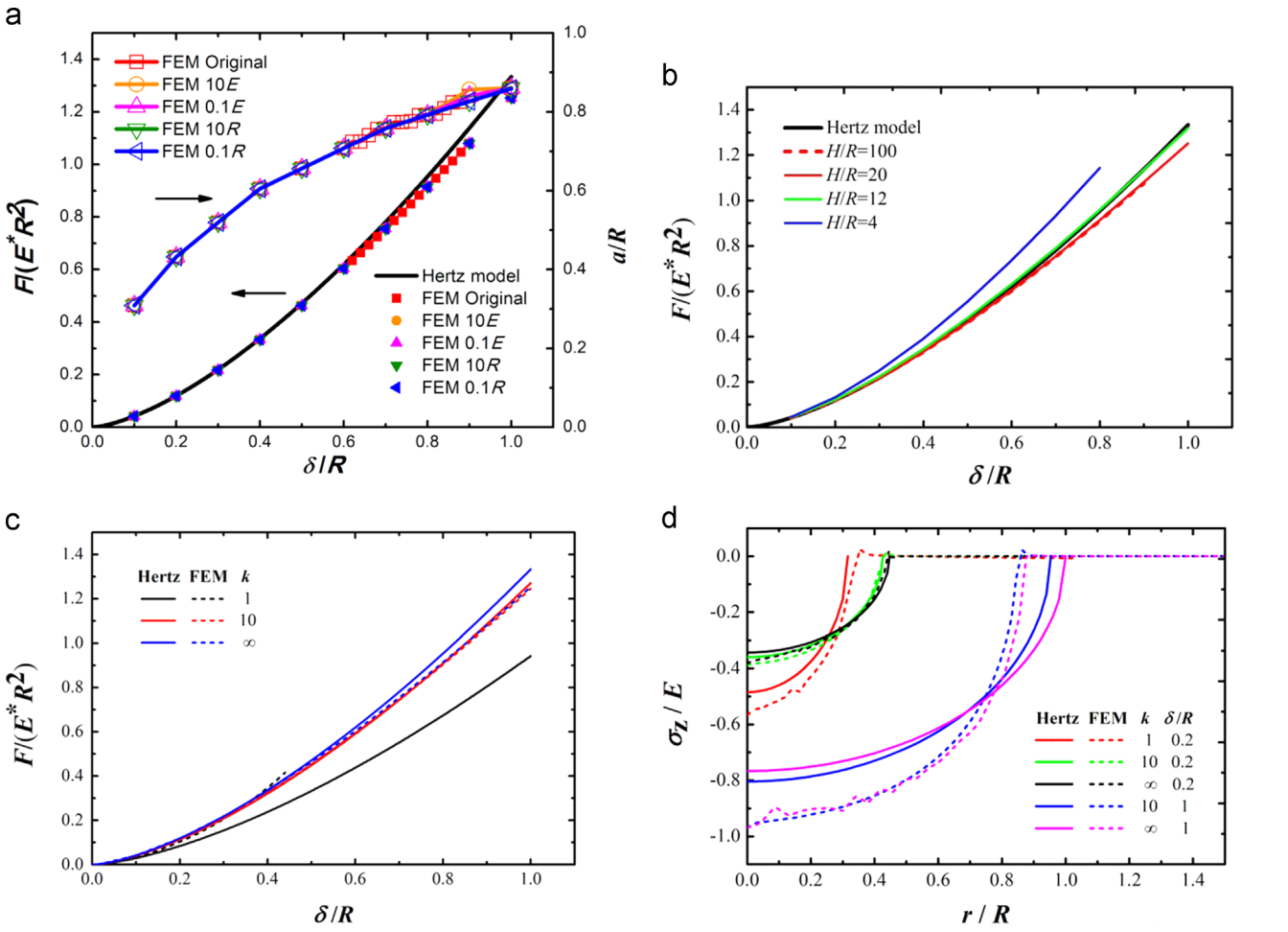

Fig. 6. (a) Dimensionless load, contact radius, and maximum principal strain versus dimensionless displacement at different elastic moduli and indenter radii. (b) Dimensionless load versus dimensionless displacement for finite substrates with different thickness H. (c) Dimensionless load versus dimensionless displacement for indenting an elastic sphere with radius kR. (d) Comparison of dimensionless contact pressure and contact radius between the Hertz theory and FEM.

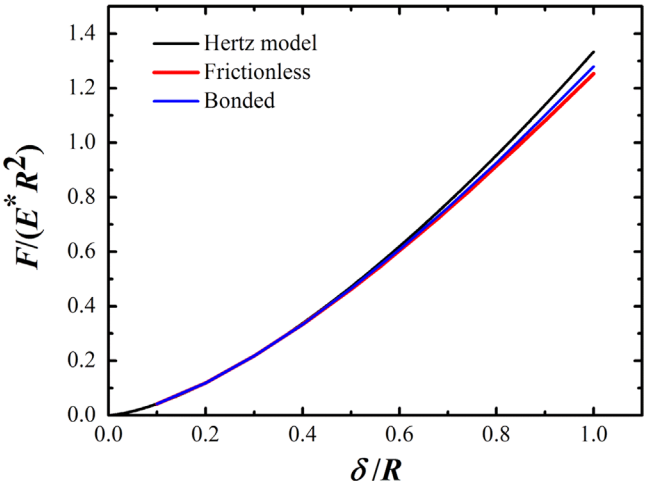

Fig. 7. Comparison of the dimensionless load versus dimensionless displacement between Eq. (1), frictionless contact interface (FEM), and bonded contact interface (FEM). The interfacial friction has minimum effect on the loading curve, indicating that the discrepancy is not due to the non-zero interfacial friction, and our results still hold regardless of the local friction coefficient.

We now consider rigid spherical indentation on an elastic sphere with a radius of kR. Results of different radii are shown in Fig. 6(c). The loads predicted by Eq. (1) and FEM show an opposite trend versus k, which can also be attributed to the effect of rigid support. As k becomes smaller, the elastic sphere may no longer be assumed semi-infinite, and the influence of the rigid support becomes apparent. Eq. (1) does not include this effect, and hence underestimates the load when indenting smaller spheres. Two important observations are made here. First, the curves of FEM of $k=10$ and $k=\infty$ (half-space) are very close, implying that the elastic sphere is large enough to be treated as a half-space for $k>10$. Second, at $k=10$ the FEM curve coincides with Eq. (1) up to $\delta/R=1$ (deviation is 2% at $\delta/R=1$). A closer look at the pressure distributions in Fig. 6(d) reveals that the Hertz theory overestimates the contact radius and underestimates the peak contact pressure, compared with the FEM, at $k=10$ and $\delta/R=1$, but their resultants happen to be the same.

5. Conclusion

In conclusion, we conducted nanoindenation tests and FEM simulations to demonstrate that the Hertzian load–displacement relation holds for rigid spherical indentation on an elastic half-space undergoing large indentations. The deviation in load is less than 3% at an indenter displacement of $\delta/R=0.66$ ($a/R=0.74$ and maximum principal strain=46.6%). This agreement arises from a near cancellation of two non-Hertzian effects: the spherical (as opposed to paraboloidal) shape of the indenter, and the large deformation behavior of the linear elastic system. When the substrate thickness is reduced to $H/R=20$ and can no longer be

regarded as a half-space, Eq. (1) happens to be in excellent agreement with the FEM results up to $\delta/R=1$ due to the rigid support at the bottom of the finite substrate. We also consider rigid indentation on an elastic sphere with a radius of kR, and reveal that the elastic sphere is large enough to be treated as a half-space for $k>10$. Our results may provide useful guidelines to help design proper sample thickness and better interpret the indentation data of soft elastomers and gels.

Acknowledgment

This work is supported by the Ministry of Science and Technology, Taiwan (MOST) (102-2221-E-002-178). We thank Yi-Chia Liao for technical supports of nanoindenation and tensile tests, and Dr. Li Xu and Prof. Yuan-Fang Chou for helpful discussions.

References

[1] Luan B, Robbins MO. The breakdown of continuum models for mechanical contacts. Nature 2005;435:929–32. http://dx.doi.org/10.1038/nature03700.
[2] Suresh S. Graded materials for resistance to contact deformation and damage. Science 2001;292(80):2447–51. http://dx.doi.org/10.1126/science.1059716.
[3] Maitre J-L, Berthoumieux H, Krens SFG, Salbreux G, Julicher F, Paluch E, et al. Adhesion functions in cell sorting by mechanically coupling the cortices of adhering cells. Science 2012;338(80):253–6. http://dx.doi.org/10.1126/science.1225399.
[4] Arzt E, Gorb S, Spolenak R. From micro to nano contacts in biological attachment devices. PNAS 2003;100:10603–6. http://dx.doi.org/10.1073/pnas.1534701100.
[5] Van Zeebroeck M, Tijskens E, Dintwa E, Kafashan J, Loodts J, De Baerdemaeker J, et al. The discrete element method (DEM) to simulate fruit impact damage during transport and handling: Case study of vibration damage during apple bulk transport. Postharvest Biol Technol 2006;41:92–100. http://dx.doi.org/10.1016/j.postharvbio.2006.02.006.
[6] Dominik C, Tielens a. GGM. The physics of dust coagulation and the structure of dust aggregates in space. Astrophys J 1997;480:647–73. http://dx.doi.org/10.1086/303996.
[7] Fischer-Cripps AC. Nanoindentation. 3rd ed. New York, NY: Springer Science+Business Media, LLC; 2011.
[8] Boccaccio A, Frassanito MC, Lamberti L, Brunelli R, Maulucci G, Monaci M, et al. Nanoscale characterization of the biomechanical hardening of bovine zona pellucida. J R Soc Interface 2012;9:2871–82. http://dx.doi.org/10.1098/rsif.2012.0269.
[9] Martin CL, Bouvard D, Shima S. Study of particle rearrangement during powder compaction by the discrete element method. J Mech Phys Solids 2003;51:667–93. http://dx.doi.org/10.1016/S0022-5096(02)00101-1.
[10] Ono K. Numerical method of analyzing contact mechanics between a sphere and a flat considering lennard-jones surface forces of contacting asperities and noncontacting rough surfaces. J Tribol 2012;134:011402. http://dx.doi.org/10.1115/1.4005643.
[11] Shabana AA, Tobaa M, Sugiyama H, Zaazaa KE. On the computer formulations of the wheel/rail contact problem. Nonlinear Dyn 2005;40:169–93. http://dx.doi.org/10.1007/s11071-005-5200-y.
[12] Hertz H. Ueber die Berührung fester elastischer Körper. J Für Die Reine Und Angew Math 1882;92:156–71.
[13] Lin DC, Shreiber DI, Dimitriadis EK, Horkay F. Spherical indentation of soft matter beyond the Hertzian regime: numerical and experimental validation of hyperelastic models. Biomech Model Mechanobiol 2009;8:345–58. http://dx.doi.org/10.1007/s10237-008-0139-9.
[14] Liu DX, Zhang ZD, Sun LZ. Nonlinear elastic load–displacement relation for spherical indentation on rubberlike materials. J Mater Res 2010;25:2197–202. http://dx.doi.org/10.1557/jmr.2010.0285.
[15] Zhang M-G, Cao Y-P, Li G-Y, Feng X-Q. Spherical indentation method for determining the constitutive parameters of hyperelastic soft materials. Biomech Model Mechanobiol 2014;13:1–11. http://dx.doi.org/10.1007/s10237-013-0481-4.
[16] Johnson K. One hundred years of Hertz contact. Proc Inst Mech Eng 1982;196:363–78. http://dx.doi.org/10.1243/PIME.
[17] Johnson KL. Contact mechanics. Cambridge, UK: Cambridge University Press; 1985.
[18] Cross SE, Jin Y-S, Rao J, Gimzewski JK. Nanomechanical analysis of cells from cancer patients. Nat Nanotechnol 2007;2:780–3. http://dx.doi.org/10.1038/nnano.2007.388.
[19] Xu W, Chahine N, Sulchek T. Extreme hardening of PDMS thin films due to high compressive strain and confined thickness. Langmuir 2011;27:8470–7. http://dx.doi.org/10.1021/la201122e.
[20] Vu-Quoc L, Zhang X. An elastoplastic contact force-displacement model in the normal direction: displacement-driven version. Proc R Soc A Math Phys Eng Sci 1999;455:4013–44. http://dx.doi.org/10.1098/rspa.1999.0488.
[21] Dintwa E, Tijskens E, Ramon H. On the accuracy of the Hertz model to describe the normal contact of soft elastic spheres. Granul Matter 2008;10:209–21. http://dx.doi.org/10.1007/s10035-007-0078-7.
[22] Yoffe EH. Modified Hertz theory for spherical indentation. Philos Mag A 1984;50:813–28. http://dx.doi.org/10.1080/01418618408237539.
[23] Lim YY, Chaudhri MM. Indentation of elastic solids with rigid cones. Philos Mag 2004;84:2877–903. http://dx.doi.org/10.1080/14786430410001716782.
[24] Giannakopoulos AE, Triantafyllou A. Spherical indentation of incompressible rubber-like materials. J Mech Phys Solids 2007;55:1196–211. http://dx.doi.org/10.1016/j.jmps.2006.11.010.
[25] Huang Y, Paul DR. Effect of large deformation and material nonlinearity on the JKR test of soft elastic materials. J Polym Sci Part B Polym Phys 2006;44:2912–22. http://dx.doi.org/10.1002/polb.
[26] Chen Z, Scheffer T, Seibert H, Diebels S. Macroindentation of a soft polymer: identification of hyperelasticity and validation by uni/biaxial tensile tests. Mech Mater 2013;64:111–27. http://dx.doi.org/10.1016/j.mechmat.2013.05.003.
[27] Chen Z, Diebels S. Nanoindentation of hyperelastic polymer layers at finite deformation and parameter re-identification. Arch Appl Mech 2012;82:1041–56. http://dx.doi.org/10.1007/s00419-012-0613-9.
[28] Cheneler D, Mehrban N, Bowen J. Spherical indentation analysis of stress relaxation for thin film viscoelastic materials. Rheol Acta 2013;52:695–706. http://dx.doi.org/10.1007/s00397-013-0707-5.
[29] Chen Z, Diebels S. Indentation of PU at different scales and computational modeling: identification of viscoelasticity and quantification of adhesion effects. Arch Appl Mech 2015;85:1225–43. http://dx.doi.org/10.1007/s00419-015-1008-5.
[30] Hu Y, Zhao X, Vlassak JJ, Suo Z. Using indentation to characterize the poroelasticity of gels. Appl Phys Lett 2010;96:2009–11. http://dx.doi.org/10.1063/1.3370354.
[31] Nalam PC, Gosvami NN, Caporizzo MA, Composto RJ, Carpick RW. Nano-rheology of hydrogels using direct drive force modulation atomic force microscopy. Soft Matter 2015;11:8165–78. http://dx.doi.org/10.1039/C5SM01143D.
[32] van Noort R, Bayston R. Mechanical properties of antibacterial silicone rubber for hydrocephalus shunts. J Biomed Mater Res 1979;13:623–30. http://dx.doi.org/10.1002/jbm.820130408.
[33] Style RW, Hyland C, Boltyanskiy R, Wettlaufer JS, Dufresne ER. Surface tension and contact with soft elastic solids. Nat Commun 2013;4:2728. http://dx.doi.org/10.1038/ncomms3728.
[34] Schneider F, Fellner T, Wilde J, Wallrabe U. Mechanical properties of silicones for MEMS. JMM 2008;18:065008. http://dx.doi.org/10.1088/0960-1317/18/6/065008.
[35] Sirghi L, Rossi F. Adhesion and elasticity in nanoscale indentation. Appl Phys Lett 2006;89:243118. http://dx.doi.org/10.1063/1.2404981.
[36] Chaudhury MK, Whitesides GM. Direct measurement of interfacial interactions between semispherical lenses and flat sheets of poly(dimethylsiloxane) and their chemical derivatives. Langmuir 1991;7:1013–25. http://dx.doi.org/10.1021/la00053a033.
[37] Pharr G, Oliver W. Measurement of thin film mechanical properties using nanoindentation. MRS Bull 1992;17:28–33. http://dx.doi.org/10.1557/S0883769400041634.